Acta Biomaterialia 8 (2012) 282–288

Contents lists available at SciVerse ScienceDirect

Acta Biomaterialia

journal homepage: www.elsevier.com/locate/actabiomat

Effect of nano- and micro-roughness on adhesion of bioinspired micropatterned surfaces

Natalia Cañas [a], Marleen Kamperman [b,*], Benjamin Völker [c], Elmar Kroner [a], Robert M. McMeeking [a,c,d,e], Eduard Arzt [a]

[a] INM – Leibniz Institute for New Materials, Functional Surfaces Group and Saarland University, Campus D2 2, 66123 Saarbrücken, Germany
[b] Wageningen University, Physical Chemistry and Colloid Science, Dreijenplein 6, 6703 HB Wageningen, The Netherlands
[c] Department of Mechanical Engineering, University of California, Santa Barbara, CA 93106, USA
[d] Materials Department, University of California, Santa Barbara, CA 93106, USA
[e] School of Engineering, University of Aberdeen, King's College, Aberdeen AB24 3UE, UK

ARTICLE INFO

Article history:
Received 7 June 2011
Received in revised form 18 August 2011
Accepted 31 August 2011
Available online 6 September 2011

Keywords:
Dry adhesion
Micropatterned surfaces
Gecko
Surface roughness
Bioinspiration

ABSTRACT

In this work, the adhesion of biomimetic polydimethylsiloxane (PDMS) pillar arrays with mushroom-shaped tips was studied on nano- and micro-rough surfaces and compared to unpatterned controls. The adhesion strength on nano-rough surfaces invariably decreased with increasing roughness, but pillar arrays retained higher adhesion strengths than unpatterned controls in all cases. The results were analyzed with a model that focuses on the effect on adhesion of depressions in a rough surface. The model fits the data very well, suggesting that the pull-off strength for patterned PDMS is controlled by the deepest dimple-like feature on the rough surface. The lower pull-off strength for unpatterned PDMS may be explained by the initiation of the pull-off process at the edge of the probe, where significant stress concentrates. With micro-rough surfaces, pillar arrays showed maximum adhesion with a certain intermediate roughness, while unpatterned controls did not show any measurable adhesion. This effect can be explained by the inability of micropatterned surfaces to conform to very fine and very large surface asperities.

1. Introduction

Many insect and lizard species possess adhesive organs on their feet that allow them to adhere to a wide variety of surfaces. The key strategy to control adhesion in these natural systems is the incorporation of fibrillar structures [1–6]. In the particular case of the gecko foot, each fibril or seta is ~100 μm long, has a diameter of a few microns and branches into an array of hundreds of spatula structures. These structures terminate in a triangular plate tip with dimensions of ~0.2 μm in length and a thickness of 10 nm [1]. The gecko uses non-covalent surface forces to achieve adhesion, which relies primarily on van der Waals forces [7].

Because the strength of van der Waals forces strongly decreases with increasing distance between the surfaces, an important aspect in adhesion is the true area of contact. Although surface area is increased by the surface roughness, more elastic strain energy is needed for the adhesion structure to conform to the rough surfaces and make contact. Macroscopic solids normally do not adhere on rough surfaces; a root-mean-square (RMS) roughness of ~1 μm is sufficient to result in negligible adhesion between rubber and a hard flat surface [8]. For purely elastic materials, only very compliant materials (Young's modulus E ~100 kPa) can adhere well on hard rough surfaces, because the elastic energy stored during deformation of the compliant material is low compared to the energy gained by forming a contact [8,9].

Geckos show high adhesion to rough surfaces in spite of the stiff structural material (β-keratin: E ~1 GPa) [10–12]. In this case adhesion is possible, because the hierarchical build-up of the fibrillar structure results in a low effective modulus and allows conformation to rough surfaces by fiber bending and buckling [5,8,13–15]. Despite the ability of geckos to conform to rough surfaces, observations of living geckos show that adhesion strongly decreases for certain roughness values [10–12]. This may explain why geckos seem to have an over-redundant attachment system [16].

Significant decreases in adhesion were also found in the few studies published on biomimetic adhesives using technologically relevant rough surfaces [17–19] or model surfaces with well-defined roughness [19,20]. In all cases, the adhesion decreased with increasing roughness [19,20] and hierarchical structures outperformed single-level structures, but only on rough surfaces [18,20].

* Corresponding author. Tel.: +31 (0)317 482358; fax. +31 (0)317 483777.
E-mail address: marleen.kamperman@wur.nl (M. Kamperman).

1742-7061/$ - see front matter © 2011 Acta Materialia Inc. Published by Elsevier Ltd. All rights reserved.
doi:10.1016/j.actbio.2011.08.028

In this work we study the adhesion of polydimethylsiloxane (PDMS) pillar arrays with mushroom-shaped tips on "nano-rough" and "micro-rough" surfaces. These surfaces have RMS roughness values in the nano- and micro-range, respectively. PDMS pillar arrays were fabricated by molding on lithographic molds and roughened Si wafers and sandpaper substrates were used as counter surfaces in adhesion measurements. The results provide new insights on the effects of roughness on the nano- and the micron scale on adhesion of patterned surfaces.

2. Materials and methods

2.1. Sample fabrication

Micropatterned structures were fabricated by demolding PDMS (Sylgard 184, Dow Corning, USA) from structured templates. SU-8 templates (SU-8 from Micro Resist Technology, Berlin, Germany; Si wafers from Crystec Berlin, Germany) with holes of different radii and lengths were obtained by a modified photolithography technique, in which quenching was used to control the pillar tip shape. Process parameters can be found in previous publications [21,22]. Quenching the template, i.e. rapid cooling from 90 °C to room temperature after the photoresist hard-baking step, caused delamination of the SU-8 at the edges of the holes. Silanization with hexadecafluoro-1,1,2,2-tetrahydrooctyltrichlorosilane and subsequent molding PDMS on these templates resulted in pillars with a small thin cap on the tip (mushroom shape). For molding, a 10:1 ratio of Sylgard 184 prepolymer and cross-linker were mixed and degassed in a desiccator for 30 min to eliminate bubbles. The mixture was poured on the template and cured for 24 h at 75 °C and 600 mbar. PDMS samples were then carefully peeled off from the mold and characterized with light microscopy (Olympus BX51) and scanning electron microscopy (SEM) (FEI Quanta 400 ESEM operating at energy between 1 and 15 kV). Micropatterned PDMS adhesives with different pillar lengths (20 and 42 μm) and aspect ratios (length/diameter) (1 and 2) were fabricated (see Table 1). The specimens had a cross-sectional area of $8 \times 8\ mm^2$.

Fig. 1 shows representative SEM images of PDMS-1 (Fig. 1a and b), PDMS-2 (Fig. 1d) and PDMS-3 (Fig. 1c). The pillars have a ~500 nm ring around the tip (Fig. 1b), resembling a mushroom profile.

2.2. Preparation and characterization of rough surfaces

Silicon wafers and sandpaper with different roughness were selected as probe surfaces. As-received nominally flat wafers, with an RMS roughness of about 2 nm, were chosen as flat probes (probe A). Further, Si wafer pieces, with a square area of $9\ mm^2$, were roughened with diamond particles and with sandpaper. This resulted in probes with randomly distributed scratches and grooves on the surface (probes B through E). The surfaces were characterized with light microscopy (see Fig. S1 in the Supporting information) and roughness parameters were measured by white light interferometry. The RMS roughness and the peak to valley distance (PV) are listed in Table 2 and Gaussian height distributions are shown in Supporting information, Fig. S2.

Atomic force microscopy (Jeol JSPM 5200) was used to characterize the surfaces with higher resolution using smaller areas ($10\ \mu m \times 10\ \mu m$), see Fig. 2.

The sandpaper substrates (Buehler GmbH, Düsseldorf, Germany) that were used as micro-rough probes were cut into $9\ mm^2$ pieces and glued on the cantilever without further treatment. Their average particle or asperity diameters were provided by the company and are listed in Table 3.

Table 1
Micropatterned PDMS characteristics.

Sample	Length (μm)	Diameter (μm)	Aspect ratio	Tip-shape
PDMS-1	20	10	2	Mushroom
PDMS-2	20	20	1	Mushroom
PDMS-3	42	20	2	Mushroom
PDMS-unpatterned	–	–	–	–

2.3. Adhesion measurements

Adhesion measurements were performed with a home-built adhesion tester, as previously described in Ref. [23]. The PDMS samples were placed on a stage, while the probe (Si wafer or sandpaper) was glued onto the spring with cyanoacrylate glue (Cyanolube, HK Wentworth Ltd., Derbyshire). The sample was loaded against and retracted from the probe using a hexapod, i.e. a six-axis positioning system that allows controlled displacement with an accuracy of 100 nm. The deflection of the spring was measured with a laser interferometer. The cantilever stiffness was $1095\ N\ m^{-1}$ and the velocity for each measurement was $5\ \mu m\ s^{-1}$. The temperature and relative humidity (RH) were controlled during experiments and set at ~23 °C and ~50% RH. Since the measurements were performed using a flat probe, a precise alignment procedure had to be carried out to obtain representative and reproducible data [23]. The sample was scanned for maximum pull-off force values by tilting the hexapod along the *x*-axis and *y*-axis to determine the parallel configuration. When the position for maximum pull-off force was identified, the pull-off forces were measured for various compressive pre-stresses. The probe was cleaned with ethanol and brought into contact with the sample several times before the actual experiment because the pull-off force measured on PDMS is known to change with the number of contact formations [23].

3. Results

3.1. Nano-rough surfaces

For the experiments on nano-rough probes, patterned PDMS-1 was used. Figs. 3 and 4 show the results of adhesion measurements of unpatterned and micropatterned specimens on Si surfaces with five different roughness values. In Fig. 3, the adhesion results are presented as pull-off strength values as functions of compressive pre-stresses, both of which are derived by dividing the measured force by the nominal area of the probe ($9\ mm^2$). The pull-off strength increased rapidly with increasing pre-stress and plateaued at higher pre-stresses. The highest adhesion was found on the smooth Si wafer (probe A) at a pre-stress above ~3 kPa. Fig. 4 compares adhesion of patterned and unpatterned PDMS: the adhesion strength of patterned PDMS-1 on probe A was nearly five times higher than that of unpatterned PDMS (~20 kPa). Compared to the smooth Si wafer (probe A), a decrease in adhesion by more than 75% was observed for the surface with the lowest roughness (probe B). With increasing roughness, the adhesion dropped further. In all cases, the micropatterned PDMS sample showed higher adhesion than unpatterned PDMS.

3.2. Micro-rough surfaces

Micropatterned PDMS adhesives with different pillar lengths (20 and 42 μm) and aspect ratios (1 and 2) were tested on sandpa-

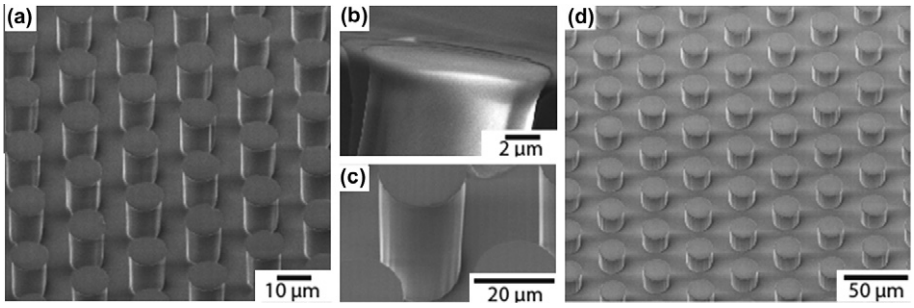

Fig. 1. SEM micrographs showing (a and b) sample PDMS-1, (c) sample PDMS-3 and (d) sample PDMS-2 obtained by demolding of PDMS from a SU-8 template.

Table 2
Roughness parameters of Si probes: RMS denotes root-mean-square roughness and PV peak-to-valley distance. The standard deviations result from three measurements on different places of the wafer. Probe A is the as-received nominally flat wafer.

Probe	RMS (nm)	PV (nm)
A	2 ± 1	23 ± 4
B	65 ± 18	638 ± 86
C	217 ± 6	3222 ± 848
D	373 ± 7	5208 ± 376
E	618 ± 32	5800 ± 1181

per with increasing asperity diameter. Fig. 5 shows the pull-off strength of patterned PDMS samples on different sandpaper substrates. It is important to note that the strength scale in Fig. 5 is in Pa, indicating a three-orders-of-magnitude decrease in adhesion relative to Fig. 3. The micropatterned surfaces all show a maximum in adhesion strength for a certain intermediate roughness. PDMS-1 did not show any adhesion to probe F, but showed low adhesion to probe G. The pull-off strength then increased for larger asperity sizes but disappeared again for probes J and K. PDMS-2 only showed adhesion to probe I. PDMS-3 required a higher compressive pre-stress to show any adhesion and only for probe J. Unpatterned PDMS showed no measureable adhesion on any of the sandpaper substrates.

In Fig. 6 the pull-off strength is plotted as a function of the compressive pre-stress. For these micro-rough surfaces the pull-off strength increases with pre-stress in a staggered manner. This is in contrast to the nano-rough surfaces, where the pull-off strength increased quickly and plateaued.

Fig. 7 shows the tensile part of the force–displacement data for PDMS-1 on probe G for different pre-stress values. The observed saw-tooth profiles, associated with isolated detachment events of pillars, differ significantly with pre-stress.

4. Discussion

4.1. Nano-rough surfaces

Micropatterned PDMS-1 showed high adhesion, with a pull-off strength exceeding 80 kPa on smooth Si wafer with an RMS roughness of 2 nm (probe A). The values were always higher than for unpatterned controls, which is in agreement with previous experimental work [21,22]. The mushroom shape of these 20 μm high pillars presumably enhances adhesion; theoretical stress analysis of differently shaped pillar tips has suggested that stress singularities are eliminated for mushrooms and defects (e.g. surface roughness, imperfections of the pillar, dirt particles) near the edge of the adhesion area are much more damaging to the pull-off strength for punch shaped pillars than for mushrooms [24,25].

We utilize a model of adhesion for a dimpled surface developed by McMeeking et al. [26] and interpret results from it to understand the interaction between a compliant, smooth surface and a rough, stiff one. We note that several researchers have previously addressed the effect that roughness has on adhesion and developed models thereof. Examples include the work of Johnson [27], Hui et al. [28], Carbone and Mangialardi [29] and Guduru [30] on adhesion involving periodically wavy surfaces. Of note is the paper by Fuller and Tabor [31] on roughness and adhesion that involves the analysis of attraction between small asperities on opposite surfaces that is mitigated by elastic interference among larger asperities on those surfaces. In addition, Hui et al. [32] use similar concepts to model the effect of roughness on adhesion, but with a focus on the interaction among neighboring fibrils. It follows that some understanding of the effect of roughness on adhesion that is relevant to our experimental work can be gleaned from the model of Fuller and Tabor [31], and from features of the analysis carried out by Johnson [27] and Hui et al. [28]. We comment on those insights below, but prefer to develop a very simple model for roughness utilizing the dimple concept [26], as it concentrates on the effect on adhesion of depressions in a rough surface rather than asperities. As such our model provides an alternative view of the effect of roughness on adhesion compared to previous work.

We assume that the work of adhesion, W, controls attachment and detachment. Roughness is represented by the characteristics of a single, isolated dimple, on the rationale that detachment will commence at such a feature and grow unstably. This concept implies that the dimple that triggers the detachment is a relatively deep one that will initiate detachment quite easily. However, we use average measures of the roughness to characterize the initiation of detachment from the dimple on the rationale that the dimensions of the most severe dimple will scale with the average roughness.

Now consider the effect of a dimple on the surface of a stiff material when it is in contact with the flat surface of a compliant material. If the dimple is shallow and small, and the deformable material compliant, or if the adhesion energy is large, intimate contact of the adhering surfaces will be formed within the dimple when they are brought together; it will then be relatively difficult to initiate detachment within the dimple when the surfaces are pulled apart. If the dimple is deep and large, the deformable surface stiff, or if the adhesion energy is low, the two surfaces will not adhere completely within the dimple; where it is deepest there will be a gap between the two surfaces when they are brought into contact. In this situation, it will be easier to initiate detachment as the gap will act as an adhesion defect, and the adhesion strength will be weakened. Furthermore, the adhesion strength will vary inversely with the dimple depth and size. As McMeeking et al. [26] have noted, the regimes just described are divided in parameter space at the value $\delta_0{}^2E^*/bW = 2\pi$, where δ_0 is the depth of the dimple, b is its radius and

$$\frac{1}{E^*} = \frac{1-\nu_1^2}{E_1} + \frac{1-\nu_2^2}{E_1} \tag{1}$$

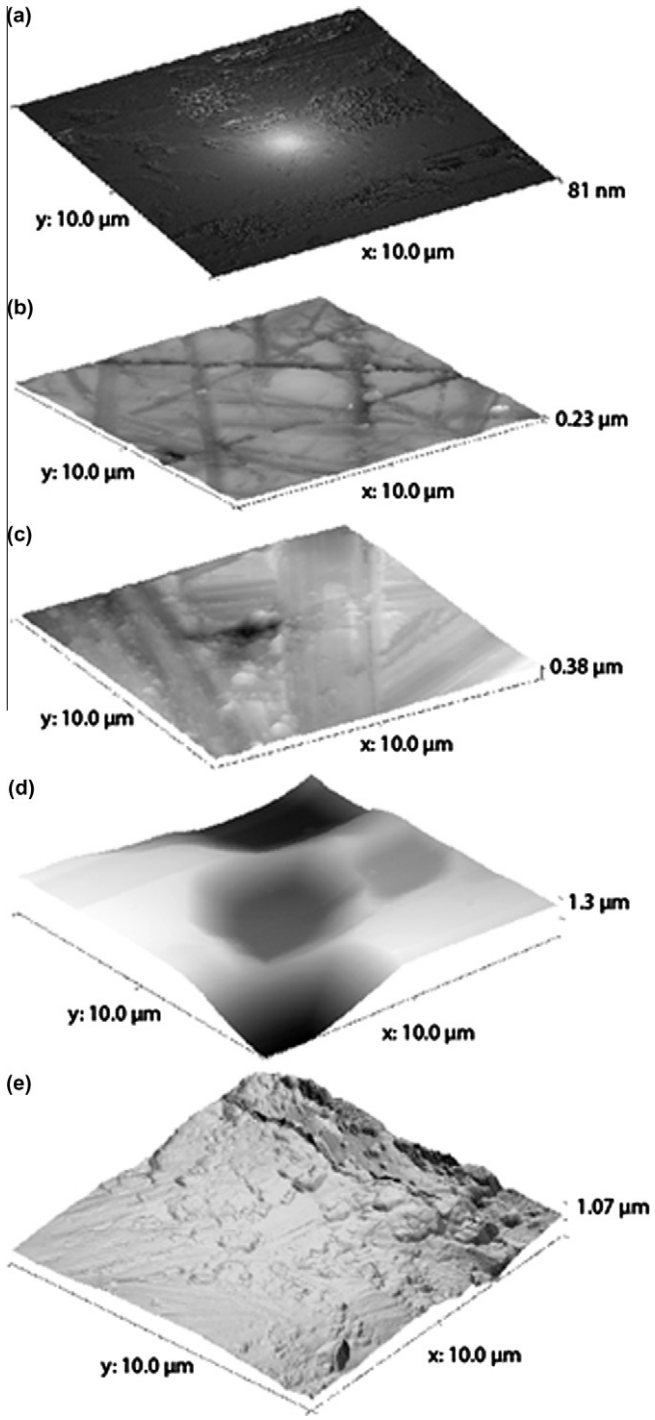

Fig. 2. Atomic force microscopy images of flat and polished probes: (a–e) probes A–E with RMS roughness values of 2, 65, 217, 373 and 618 nm, respectively.

Table 3
Sandpaper substrates used as probes for adhesion measurements.

Probe	FEPA designation[a]	Average asperity diameter (µm)
F	P4000	~5
G	P2400	~8
H	P1200	~14
I	P800	~22
J	P320	~46
K	P220	~68

[a] FEPA (Federation of European Producers of Abrasives), ISO 6344 standard.

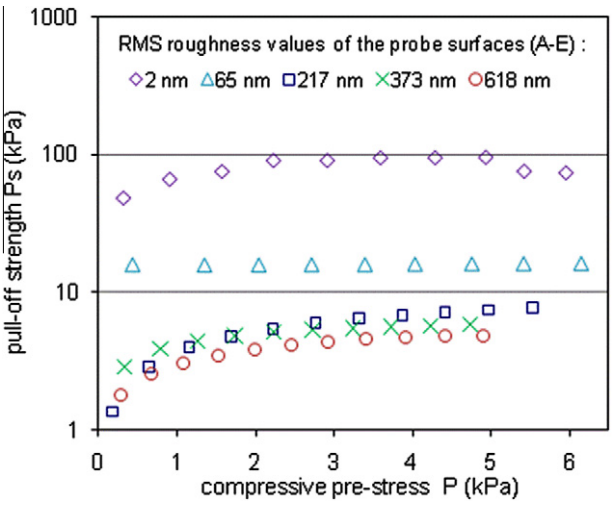

Fig. 3. Pull-off strength values for micropatterned PDMS-1 on flat and rough Si surfaces as a function of pre-stress. Different colors correspond to different RMS roughness values of the probe surface, the flat probe has an RMS value of 2 nm (compare Table 2).

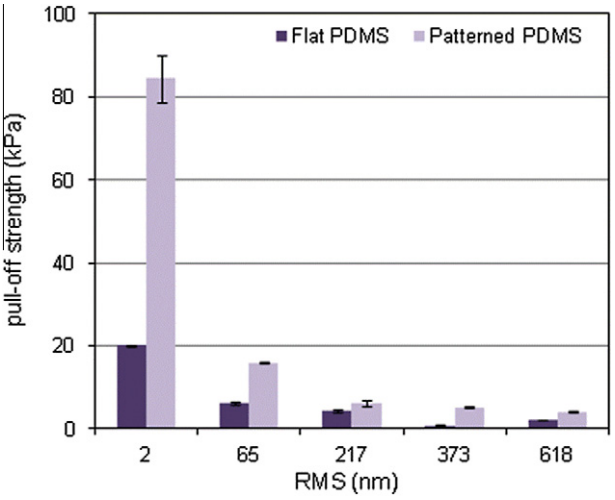

Fig. 4. Comparison of average pull-off strength values between unpatterned and micropatterned PDMS on Si probes for pre-stresses corresponding to adhesion plateaus (between 1 and 6 kPa).

where E_i is Young's modulus and v_i is Poisson's ratio, with the subscript denoting the values for the two different materials being brought into contact. For $\delta_0^2 E^*/bW < 2\pi$ intimate contact will always be formed within the dimple even when no compression is applied. When $\delta_0^2 E^*/bW > 2\pi$ a gap within the dimple will be left between the two surfaces when no load is applied that can only be closed by application of compression.

Consider the case of a dimple having $\delta_0 = b$ and $\delta_0^2 E^*/bW > 2\pi$. We assume that any compression previously applied was insufficient to close the gap between the adhering surfaces, and it remains at the bottom of the dimple. When tension is applied to the system, the gap stably enlarges until the defect reaches a critical diameter at which it becomes unstable. Thereafter the detachment then extends unstably and the two surfaces separate. This occurs at a critical stress computed by McMeeking et al. [26] as

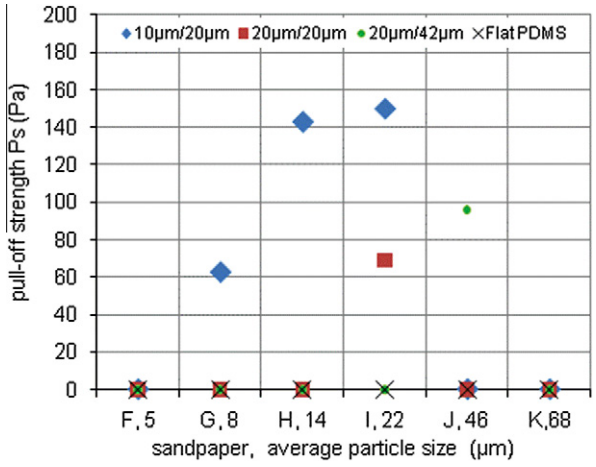

Fig. 5. Comparison of the pull-off strength for patterned PDMS samples on sandpaper substrates F to K. The pull-off strength was determined at compressive pre-stresses between 2 and 3.5 kPa. PDMS-3 required a higher pre-stress (6–7.5 kPa) to show adhesion. Unpatterned specimens exhibited no measureable adhesion.

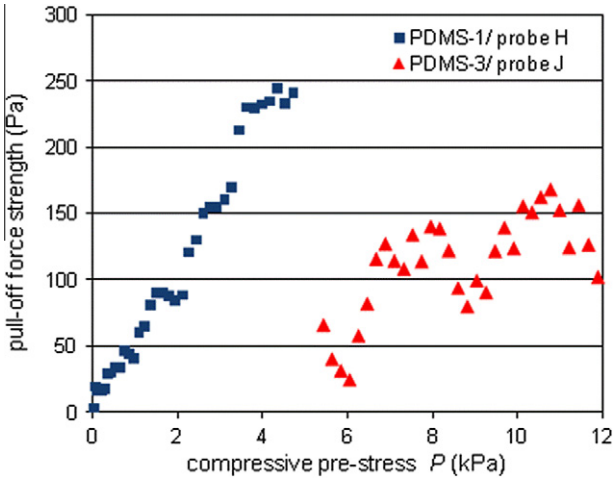

Fig. 6. Dependence of pull-off strength on pre-stress for two micropatterned PDMS surfaces on sandpaper.

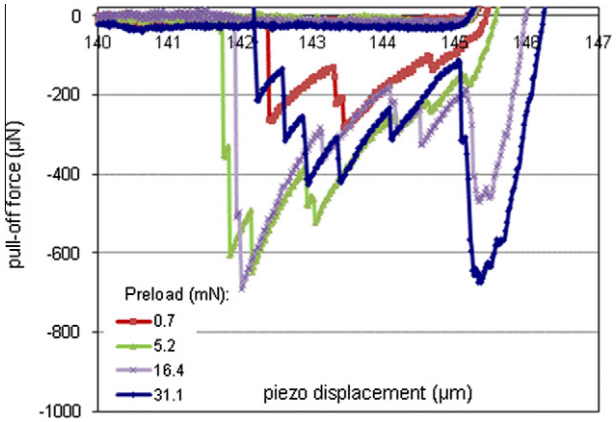

Fig. 7. Representative force displacement curves for PDMS-1 on probe G.

$$\sigma_p = E^*\left[\sqrt{\frac{\pi W}{2aE^*}} - \frac{1}{2}\left(1 - \sqrt{1 - \frac{\delta_0^2}{a^2}}\right)\right]$$

$$\frac{a}{\delta_0} = \left[\frac{E^*\delta_0}{\pi W} + \sqrt{\left(\frac{E^*\delta_0}{\pi W}\right)^2 - \frac{1}{27}}\right]^{\frac{1}{3}} + \left[\frac{E^*\delta_0}{\pi W} + \sqrt{\left(\frac{E^*\delta_0}{\pi W}\right)^2 - \frac{1}{27}}\right]^{\frac{1}{3}} \quad (2)$$

where a is the radius of the circular gap when it becomes unstable. The parameter σ_p is therefore the adhesion strength, and we use δ_0 to represent the root mean square roughness.

In Fig. 8 we plot σ_p/E^* vs. $E^*\delta_0/W$ from Eq. (2). Thereafter in Fig. 9 we have fitted the function in Fig. 8 to the data for pull-off stress for patterned PDMS surfaces summarized in Table 4. The parameters used to obtain our least squares fit, after allowing for the area fraction of fibrils of 0.227 on the patterned surfaces, imply that $E^* = 25$ kPa and $W = 1.6$ mJ m^{-2}. We note that the value of the effective elastic modulus implied by our fit to the data is rather low compared to typical values for this parameter of around 1–2 MPa. Similarly, the value of the adhesion energy implied by the fit to the data is low, but in better agreement than the modulus, since typical values for the adhesion energy for PDMS against Si are ~45 mJ m^{-2}.

Under these assumptions, the fit is very good, suggesting that the pull-off strength for patterned PDMS is controlled by the deepest dimple-like features on the rough surface. Note that the fitting procedure included the use of the data for the RMS roughness of 2 nm. It is dubious whether dimple-like features control pull-off when the RMS roughness is as low as 2 nm, but it made negligible difference to the fitting parameters whether the data for RMS roughness equal to 2 nm were included in the fitting procedure or not. Thus, the question of whether dimple-like features control pull-off for such small roughness is difficult to address, and it is uncertain whether pull-off in this case is initiated at the edge of the fibrils instead. In contrast, it seems more likely that the pull-off process for unpatterned PDMS samples is initiated at the edge of the probe where significant stress concentrations will be found. Perhaps this explains the much lower pull-off strength observed for unpatterned PDMS samples, and features of the roughness at this edge can be presumed to control the pull-off strength for flat, unpatterned PDMS.

We note that the model of Fuller and Tabor [31] also leads to the prediction that the pull-off strength varies inversely with the surface roughness, and is thus viable for rationalizing the data from our experiments. However, their model uses Johnson et al. [33] concepts, implying that only a small fraction of the area of the two surfaces has mutual contact, a situation that seems unlikely when one of the materials is very compliant as in the case of PDMS. In addition, some of the features of the behavior analyzed for the models for adhesion between periodically wavy surfaces presented by Johnson [27] and Hui et al. [28] are relevant to the phenomena we are addressing; these aspects include the observation [27] that the two surfaces can spontaneously adhere perfectly without gaps if one or other or both of the materials are sufficiently compliant, and the fact that unstable separation can be achieved if a sufficiently high tensile stress is applied. Nevertheless, we believe that our simple model using the concept of a dimple to represent the roughness brings these and other features out quite clearly, and provides a useful model for the effect of roughness on the adhesion between two bodies.

4.2. Micro-rough surfaces

The low adhesion strengths shown in Fig. 5 indicate that the non-hierarchical patterned structures used in this study do not perform well on micro-rough surfaces. Although micropatterned surfaces have smaller effective elastic moduli and pillars may bend and

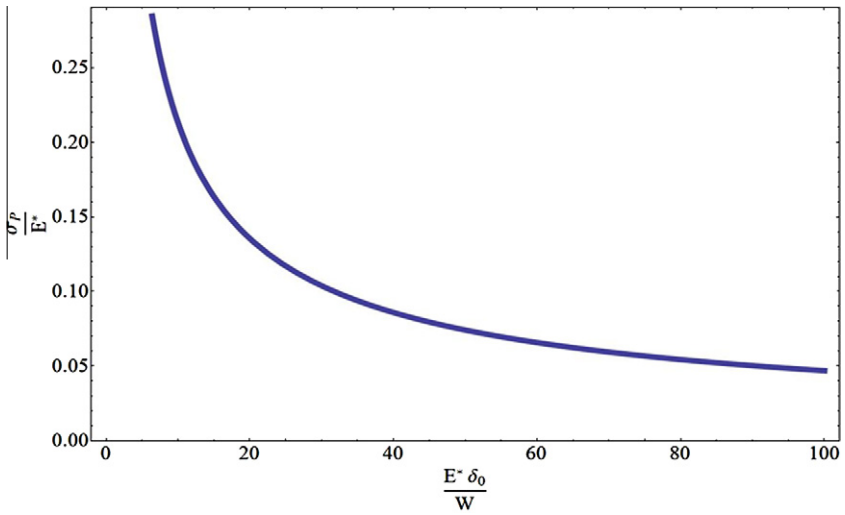

Fig. 8. Plot of the adhesion strength, σ_p, normalized by the effective joint elastic modulus, E^*, vs. the surface roughness parameter, $E^*\delta_0/W$, where δ_0 is the RMS surface roughness and W is the adhesion energy. The plot depicts the prediction from Eq. (2).

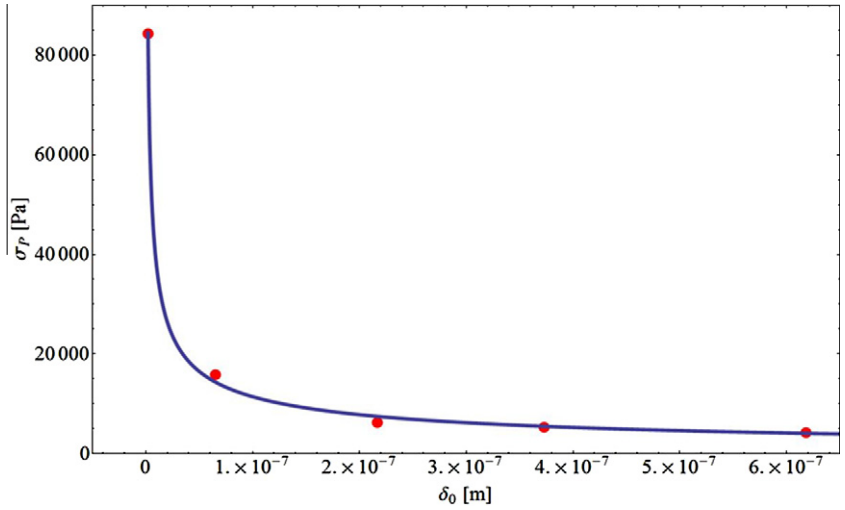

Fig. 9. Least squares fit of the predicted adhesion strength, σ_p, from Eq. (2) to experimental data for pull-off stress shown in Table 1, where δ_0 is the RMS surface roughness.

Table 4
Experimental data used as input for least square fit of Eq. (2).

RMS roughness [nm]	2	65	217	373	618
pull-off stress [kPa]	84.3	15.9	6.2	5.3	4.2

buckle to form contact with the rough surface, the elastic energy penalty is seemingly too high. Nonetheless, the adhesion strengths of the micropatterned surfaces display an interesting dependence on micro-roughness. PDMS-1 showed a maximum in adhesion on probe I and no adhesion on the finest (probe F) and the coarsest (probe J) sandpaper. The loss of adhesion of PDMS-1 on probe F may be due to the relatively large size of the pillar diameter (10 μm) with respect to the average asperity size of the sandpaper (5 μm). The pillars may not be able to penetrate into the valleys and make close contact with the probe, resulting in no measureable adhesion strength. For larger asperity sizes, the adhesion strength

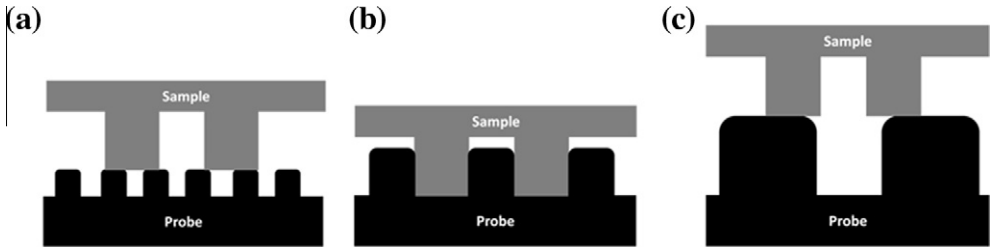

Fig. 10. Schematic explanation of adhesion loss for pillar arrays on micro-rough surfaces: (a) when the asperity size is much smaller than the pillar dimensions, the pillars cannot penetrate into the valleys between the asperities, resulting in low adhesion; (b) adhesion is enhanced when the pillar dimensions and the average asperity size of the substrate coincide; and (c) for even larger asperities, pillars cannot adapt well to the substrate, resulting again in loss of adhesion.

increases, because the center-to-center distance of the asperities increases and therefore the pillars can better adapt to the micro-cavities of the probe. Therefore, a higher contact area is reached than for lower asperity sizes. This contact area includes contact of the sides of the pillar with the probe. No adhesion is possible on much larger asperities (46 and 68 μm) than the length of the pillar (20 μm). This is schematically represented in Fig. 10. As anticipated, for samples with larger diameter pillars (PDMS-2 and PDMS-3) adhesion is found only on surfaces with larger asperities.

As the pillars are pushed onto a rough surface, contact is made first with the more elevated regions. When the pre-stress increases, pillars and backing layer deform and the pillars can penetrate deeper into the valleys of the sandpaper. This may explain the high dependence of the pull-off strength on pre-stress as shown in Fig. 6. Moreover, the saw-tooth patterns of the force–displacement curves typically obtained for the measurements on sandpaper (Fig. 7) indicate discontinuous detachment of the pillars from the lowest to the highest point of the rough surface.

5. Conclusion

In this work the influence of nano- and micro-roughness on the adhesion of biomimetic micropatterned PDMS structures was studied. The following conclusions can be drawn.

Nano-roughness decreases the adhesion strength of micropatterned PDMS surfaces, but pillar arrays retained higher adhesion strengths than unpatterned controls in all cases. A model of adhesion for a dimpled surface describes the obtained strong decrease in adhesion strength at small surface roughness for patterned PDMS very well and indicates that the pull-off is controlled by the deepest depression on the rough surface. On the other hand, the pull-off strength for unpatterned PDMS may be controlled by features at the probe edge, where significant stress concentrations are found, explaining the much lower pull-off strength of unpatterned specimens in comparison with patterned specimens.

Micropatterned PDMS surfaces exhibit much lower or no adhesion to micro-rough surfaces. Nonetheless, when adhesion is present, it is found to display an interesting dependence on micro-roughness: a maximum in adhesion for a certain intermediate roughness, close to the pillar dimensions, was obtained. Our study suggests that micropatterned surfaces are unable to conform to very fine and very large surface asperities, resulting in poor contact formation.

Acknowledgements

Joachim Blau is acknowledged for help with the adhesion tester, Graciela Castellanos for providing the templates to fabricate the mushroom shaped PDMS adhesives, Birgit Heiland for help with the polishing experiments, Andreas Schneider and Dadhichi Paretkar for the scanning electron microscopy images and Harald Tlatlik for the atom force microscopy images. We thank Martin Müser for helpful comments on the Master thesis by N. Cañas, on which the manuscript is based, and Bo Persson for helpful discussions. This work, as part of the European Science Foundation EUROCORES Program FANAS, was supported by the German Science Foundation (DFG) Grant AR201/9-1.

Appendix A. Supplementary data

Supplementary data associated with this article can be found, in the online version, at doi:10.1016/j.actbio.2011.08.028.

Appendix B. Figures with essential colour discrimination

Certain figures in this article, particularly Figs. 3–9, are difficult to interpret in black and white. The full colour images can be found in the on-line version, at doi:10.1016/j.actbio.2011.08.028.

References

[1] Autumn K, Liang YA, Hsieh ST, Zesch W, Chan WP, Kenny TW, et al. Adhesive force of a single gecko foot-hair. J Nat 2000;405:681–5.
[2] Jagota A, Bennison S. Mechanics of adhesion through a fibrillar microstructure. J Integr Comp Biol 2002;42:1140–5.
[3] Arzt E, Gorb S, Spolenak R. From micro to nano contacts in biological attachment devices. Proc Natl Acad Sci USA 2003;100:10603–6.
[4] Gao HJ, Yao HM. Shape insensitive optimal adhesion of nanoscale fibrillar structures. Proc Natl Acad Sci USA 2004;101:7851–6.
[5] Glassmaker NJ, Jagota A, Hui CY, Kim J. Design of biomimetic fibrillar interfaces: 1. Making contact. J Roy Soc Interface 2004;1:23–33.
[6] Kamperman M, Kroner E, del Campo A, McMeeking RM, Arzt E. Functional adhesive surfaces with "Gecko" effect: the concept of contact splitting. Adv Eng Mater 2010;12:335–48.
[7] Autumn K, Sitti M, Liang YCA, Peattie AM, Hansen WR, Sponberg S, et al. Evidence for van der Waals adhesion in gecko setae. Proc Natl Acad Sci USA 2002;99:12252–6.
[8] Persson BNJ. Biological adhesion for locomotion: basic principles. J Adhes Sci Technol 2007;21:1145–73.
[9] Castellanos G, Arzt E, Kamperman M. Effect of viscoelasticity on adhesion of bioinspired micropatterned epoxy surfaces. Langmuir 2011;27(12):7752–9.
[10] Huber G, Gorb S, Hosoda N, Spolenak R, Arzt E. Influence of surface roughness on gecko adhesion. Acta Biomater 2007;3:607–10.
[11] Russell AP, Johnson MK. Real-world challenges to, and capabilities of, the gekkotan adhesive system: contrasting the rough and the smooth. Can J Zool 2007;85:1228–38.
[12] Pugno NM, Lepore E. Observation of optimal gecko's adhesion on nanorough surfaces. Biosystems 2008;94:218–22.
[13] Autumn K, Majidi C, Groff RE, Dittmore A, Fearing R. Effective elastic modulus of isolated gecko setal arrays. J Exp Biol 2006;209:3558–69.
[14] Persson BNJ. On the mechanism of adhesion in biological systems. J Chem Phys 2003;118:7614–21.
[15] Persson BNJ, Gorb S. The effect of surface roughness on the adhesion of elastic plates with application to biological systems. J Chem Phys 2003;119:11437–44.
[16] Irschick DJ, Herrel A, Vanhooydonck B. Whole-organism studies of adhesion in pad-bearing lizards: creative evolutionary solutions to functional problems. J Comp Physiol 2006;192:1169–77.
[17] Davies J, Haq S, Hawke T, Sargent JP. A practical approach to the development of a synthetic Gecko tape. Int J Adhes Adhes 2009;29:380–90.
[18] Asbeck A, Dastoor S, Parness A, Fullerton F, Esparza N, Soto D, et al. Climbing rough vertical surfaces with hierarchical directional adhesion. ICRA 2009;1–7:4328–33.
[19] Vajpayee S, Jagota A, Hui CY. Adhesion of a fibrillar interface on wet and rough surfaces. J Adhes 2010;86:39–61.
[20] Jeong HE, Lee JK, Kim HN, Moon SH, Suh KY. A nontransferring dry adhesive with hierarchical polymer nanohairs. Proc Natl Acad Sci USA 2009;106:5639–44.
[21] Greiner C, del Campo A, Arzt E. Adhesion of bioinspired micropatterned surfaces: effects of pillar radius, aspect ratio and preload. Langmuir 2007;23:3495–502.
[22] del Campo A, Greiner C, Arzt E. Contact shape controls adhesion of bioinspired fibrillar surfaces. Langmuir 2007;23:10235–43.
[23] Kroner E, Maboudian R, Arzt E. Adhesion characteristics of PDMS surfaces during repeated pull-off force measurements. Adv Eng Mater 2010;12:398–404.
[24] Spuskanyuk AV, McMeeking RM, Deshpande VS, Arzt E. The effect of shape on the adhesion of fibrillar surfaces. Acta Biomater 2008;4:1669–76.
[25] Shah GV, Sitti M. Modeling and design of biomimetic adhesives inspired by gecko foot-hairs. In: IEEE international conference on robotics and biomimetics (ROBIO), Shenyang, China; 2004. p. 873–8.
[26] McMeeking RM, Ma L, Arzt E. Bi-stable adhesion of a surface with a dimple. Adv Eng Mater 2010;12:389–97.
[27] Johnson KL. The adhesion of two elastic bodies with slightly wavy surfaces. Int J Solids Struct 1995;32:423–30.
[28] Hui CY, Lin YY, Baney JM, Kramer EJ. The mechanics of contact and adhesion of periodically rough surfaces. J Polym Sci B Polym Phys 2001;39:1195–214.
[29] Carbone G, Mangialardi L. Adhesion and friction of an elastic half-space in contact with a slightly wavy surface. J Mech Phys Solids 2004;52:1267–87.
[30] Guduru PR. Detachment of a rigid solid from an elastic wavy surface: theory. J Mech Phys Solids 2007;55:445–72.
[31] Fuller KNG, Tabor D. The effect of surface roughness on the adhesion of elastic solids. Proc R Soc Lond A 1975;345:327–42.
[32] Hui CY, Glassmaker NJ, Jagota A. How compliance compensates for surface roughness in fibrillar adhesion. J Adhes 2005;81:699–721.
[33] Johnson KL, Kendall K, Roberts AD. Surface energy and the contact of elastic solids. Proc R Soc Lond A 1971;324:301–13.